



# A Poisson-Gaussian Noise Limited Quantum Iterative Multi-User System With Non-Ideal Photon-Counting Receiver

Weiqliang Weng, Xiaolin Zhou , *Member, IEEE*, Jun Zhang , Pengfei Tian , *Member, IEEE*, Yongkang Chen, Abu Bakar Waqas, and Zhichao Dong

**Abstract**—Coherent state quantum communication is attracting extensive attention for its great value in terrestrial and satellite information networks. This paper proposes a new non-orthogonal quantum multi-user (MU) iterative detection scheme. At the receiving end, we develop a composite quantum receiver with multi-stage measurement instrument and soft iterative MU detector. Furthermore, based on a three-dimensional factor graph, a nonlinear Poisson-Gaussian noise limited coherent state iterative MU parallel interference cancellation (PIC) algorithm is derived. Our results demonstrate that this system can well support MU communication and achieve good performance. Quantitatively, for the 8 users scenario, the BER of  $10^{-6}$  can be obtained when the photon number is 19. Further numerical results show that the system we designed exhibits superior robustness against imperfections (e.g., quantum mode mismatch and quantum thermal noise).

**Index Terms**—Coherent state, iterative PIC, poisson-gaussian noise.

## I. INTRODUCTION

QUANTUM has the characteristics of non-cloning and superposition. Under the guidance of quantum mechanics, there emerge many promising technologies, such as quantum network and quantum key distribution (QKD) [1]–[4]. Besides, quantum wireless communication (QWC) has been extensively studied due to its inherent advantages, e.g. high transmission rate and unconditional communication security. It is of great application prospect in future terrestrial and satellite networks [5]–[7].

With the growth of users, the resulting multiple access interference seriously affects the performance of the communication system. To solve this problem, a variety of schemes are developed in quantum communications [8]–[10]. In [8], a novel quantum code-division multiple-access (QCDMA) network is developed, which is suitable for any input quantum pure state.

Manuscript received September 7, 2021; revised November 14, 2021; accepted November 15, 2021. Date of publication November 19, 2021; date of current version December 6, 2021. This work was supported by the National Natural Science Foundation of China under Grant 61571135. (*Corresponding author: Xiaolin Zhou.*)

The authors are with the Key Laboratory for Information Science of Electromagnetic Waves, School of Information Science and Technology, Fudan University, Shanghai 200433, China (e-mail: 18210720074@fudan.edu.cn; zhouxiaolin@fudan.edu.cn; 20110720109@fudan.edu.cn; pftian@fudan.edu.cn; 19110720055@fudan.edu.cn; bwabu18@fudan.edu.cn; zhichaodong@ynu.edu.cn).

Digital Object Identifier 10.1109/JPHOT.2021.3129452

In [9], a quantum wireless network communication (QWNC) scheme using multi-qubit Greenberger-Horne-Zeilinger (GHZ) state is proposed, which can provide lower computational complexity than the Bell state based schemes. In [10], a QKD system that utilizes wavelength division multiple access (WDMA) is demonstrated.

In addition, photomultiplier tube (PMT) receiver has been concerned due to its ability to detect signal intensity in a wide range [11]–[13]. In [11], the achievable rate and capacity of PMT receiver are studied. The upper and lower bounds on the transmission rate of optical wireless scattering system using PMT are derived in [12]. Work in [13] proposes a new adaptive control strategy for high-speed underwater wireless optical communication with PMT receiver.

In this paper, a new non-orthogonal coherent-state iterative multi-user (MU) OWC system is proposed. More explicitly, the main contributions of this paper are outlined as follows.

- 1) Under the nonlinear Poisson-Gaussian noise model, an iterative quantum MU parallel interference cancellation (PIC) algorithm is derived. Numerical results show that the proposed system can well support MU communication and obtain superior bit error ratio (BER) performance over the conventional photon-counting MU scheme [23].
- 2) An iterative composite MU receiver is developed, which composes of quantum multi-stage measurement and soft iterative MU detector. The simulation result shows that this scheme can effectively eliminate multi-user interference and achieve good BER performance.
- 3) The proposed system exhibits good robustness against the various imperfections, e.g. quantum mode mismatch and quantum thermal noise.

The remainder of this paper is organized as follows. Section II provides the system model for the quantum MU communication scheme. Section III evaluates the BER and iterative convergence performance of the system. Finally, Section IV concludes this paper.

## II. SYSTEM MODEL

### A. Transmitter Design

As shown in Fig. 1, it's assumed that the proposed quantum iterative MU system can support  $K$  users to communicate

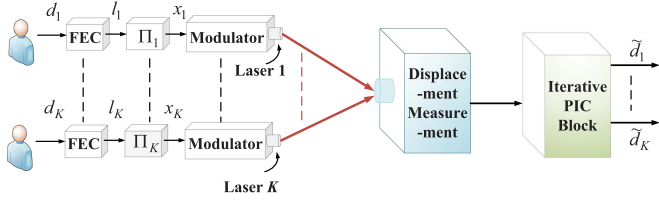


Fig. 1. The structure of quantum iterative communication for  $K$  users with composite quantum receiver, including multi-stage displacement measurement and iterative multi-user detector.

simultaneously. The transmitted information bit sequence of  $k$ th user is  $\mathbf{d}_k = \{d_k[i], i \in [1, L_d], k \in [1, K]\}$  with  $L_d$  as the length of the sequence. The sequence is then encoded with forward error correction (FEC) code, generating  $\mathbf{l}_k = \{l_k[j], j \in [1, L_c]\}$  of length  $L_c$ . After that, the chips of encoded sequence are permuted by the user-specific interleaver  $\Pi_k$ , resulting in  $\mathbf{x}_k = \{x_k[j], j \in [1, L_c]\}$ .

Quadrature amplitude modulation (QAM) is then performed on the interleaved sequence, which can be characterized by a pair of orthogonal amplitudes  $\hat{z}_c$  and  $\hat{z}_s$  in quantum theory as

$$\hat{z}_c \equiv \frac{(\hat{a} + \hat{a}^\dagger)}{2}, \quad \hat{z}_s \equiv \frac{(\hat{a} - \hat{a}^\dagger)}{2i}, \quad (1)$$

where  $\hat{a}^\dagger$  and  $\hat{a}$  are the creation and the annihilation operators respectively. Then QAM signal of coherent state is given by

$$|\alpha_{c,s}\rangle = |(c + is) \cdot \alpha\rangle, \quad c, s \in \Omega, \quad (2)$$

where  $|\alpha\rangle = e^{-\frac{1}{2}\|\alpha\|^2} \sum_{n=0}^{\infty} \frac{(\alpha)^n}{(n!)^{\frac{1}{2}}} |n\rangle$  [14].  $\alpha$  is the average number of signal photons while  $|n\rangle$  denotes the eigenstate of the number operator. Also,  $\Omega$  is the index set of the QAM symbol. When each of the two amplitudes takes  $L$  values,  $\Omega$  can be represented by

$$\Omega = \{-(L-1) + 2(w-1) | w = 1, 2, 3, \dots, L, L \\ = 2, 3, 4, 5, \dots\}. \quad (3)$$

After that, the symbol sequences are emitted to the base station with the same optical wavelength.

## B. Iterative Quantum Receiver

1) *Iterative Partition Quantum Measurement*: It can be seen from Fig. 2 that the coherent state signal at the receiving end is

$$|r[j]\rangle = \left| \sum_{k=1}^K x_k[j] \cdot \alpha \right\rangle. \quad (4)$$

The received quantum signal is firstly divided into  $Q$  consecutive partitions. This operation can be implemented by  $(Q-1)$  beam splitters (BS) with a transmittance of  $R_q$ , and the expression of  $R_q$  is

$$R_q = \frac{1}{Q-q+1}, \quad q = 1, \dots, Q-1. \quad (5)$$

The signal after partition can be denoted as  $|r_q[j]\rangle = |r[j]\rangle/\sqrt{Q}$ . Through the displacement operation  $\hat{D}(\beta)$  [15], the received signal field interferes with the local oscillator field  $|\beta_{q,m^*}[j]\rangle$ ,

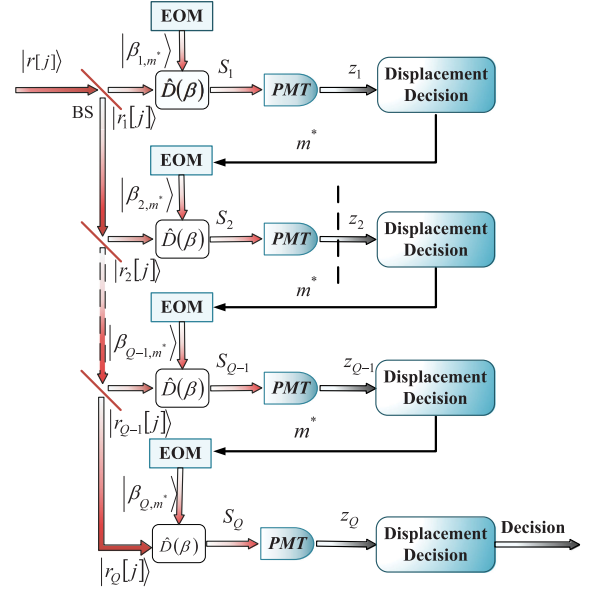


Fig. 2. The schematic of multi-stage displacement measurement for iterative receiver.

invoked for shifting the amplitude to the vicinity of the vacuum state  $|0\rangle$ . After that, PMT is used to detect the interference field and the corresponding average intensity in the  $q$ th partition can be expressed as [15]

$$S_q[j] = (1 - \vartheta) \left\| \frac{|r[j]\rangle}{\sqrt{Q}} \right\|^2 + \vartheta \left\| \frac{|r[j]\rangle}{\sqrt{Q}} - |\beta_{q,m^*}[j]\rangle \right\|^2, \quad (6)$$

where  $\vartheta$  is the quantum mode mismatch parameter between the signal field and the local oscillator field.

In the first partition, that is  $q = 1$ , it is assumed that the amplitude of the local oscillator field  $|\beta_{q,m^*}\rangle$  is any of  $M$  possible symbols, where  $M = (K+1)^2$ . In the  $q$ th ( $q > 1$ ) partition, through  $m^*$  from the previous stage, the corresponding local oscillator field is adjusted by the electro-optic modulator (EOM), i.e.  $|\beta_{q,m^*}\rangle = |r_{q,m^*}\rangle/\sqrt{Q}$  [16].  $m^*$  is obtained according to the log maximum *a posteriori* probability (Log-MAP) criterion as

$$m^* = \arg \max_{m \in [0, M]}$$

$$\times \left\{ \text{Log} \left( \frac{\Pr[|r_{q,m}[j]\rangle] \Pr[z_q[j]/|r_{q,m}[j]\rangle]}{\sum_{m=1}^M \Pr[|r_{q,m}[j]\rangle] \Pr[z_q[j]/|r_{q,m}[j]\rangle]} \right) \right\}, \quad (7)$$

where  $\Pr[|r_{q,m}[j]\rangle] = \Pr[|r_{q-1,m}[j]\rangle | z_{q-1}[j]]$  and  $q > 1$ . The output  $z_{q-1}[j]$  of PMT receiver follows the Poisson-Gaussian distribution which will be introduced in the next section. Abbreviate  $S_q[j]$  as  $S_q$ , the corresponding probability distribution function (PDF) of  $z_q[j]$  can be written as

$$\Pr(z_q[j]/S_q) \\ = \sum_{n_0=0}^{\infty} \frac{(S_q)^{n_0} \exp(-S_q)}{n_0!} \cdot G_{n_0}(z_q[j]; n_0 A e, n_0 \sigma^2 + \sigma_0^2), \quad (8)$$

and

$$G_{n_0}(z) = \frac{1}{\sqrt{2\pi(n_0\sigma^2 + \sigma_0^2)}} \cdot \exp\left(-\frac{(z - n_0Ae)^2}{2(n_0\sigma^2 + \sigma_0^2)}\right), \quad (9)$$

where  $A$  is the amplification factor,  $n_0$  denotes the number of detected photoelectrons, and  $e$  is the charge of a single electron.

After  $Q$  times of partitioned detection,  $m^*$  in the last partition is the corresponding decision output and  $\tilde{r}[j]$  could be generated according to  $m^*$ .

2) *Poisson-Gaussian Noise Model*: In this paper, a PMT receiver is used. Let  $\lambda_s$  and  $\lambda_b$  be the mean number of photoelectrons of the detected target signal portion and background noise portion, respectively. According to [17], the number of detected photoelectrons  $N_\mu$  satisfies a Poisson distribution, i.e.

$$\Pr(N_\mu = n_0) = \frac{(\lambda_s + \lambda_b)^{n_0}}{n_0!} \cdot \exp[-(\lambda_s + \lambda_b)]. \quad (10)$$

Since the PMT receiver can amplify the detected photoelectrons, we obtain

$$z = n_0Ae + v, \quad (11)$$

where  $z$  is the output signal of PMT.  $v$  represents additive Gaussian noise including thermal noise and shot noise with variances  $\sigma_0^2$  and  $\sigma^2$ , respectively. The PDF of  $z$  under detecting  $n_0$  photoelectrons is

$$\Pr(z|N_\mu = n_0) = G_{n_0}(z; n_0Ae, n_0\sigma^2 + \sigma_0^2). \quad (12)$$

Therefore, for the input signal  $(\lambda_s + \lambda_b)$ , the corresponding PDF of PMT output signal  $z$  is given as

$$\begin{aligned} \Pr(z|\lambda_s + \lambda_b) &= \sum_{n_0=0}^{\infty} \Pr(N_\mu = n_0) \cdot \Pr(z|N_\mu = n_0) \\ &= \sum_{n_0=0}^{\infty} \frac{(\lambda_s + \lambda_b)^{n_0} \cdot \exp(-\lambda_s - \lambda_b)}{n_0!} \cdot G_{n_0}(z). \end{aligned} \quad (13)$$

Based on the above, (8) can be derived by substituting  $\lambda_s + \lambda_b = S_q$  into (13).

3) *Multi-User Iterative PIC Detection*: As shown in Fig. 3, an iterative MU-PIC algorithm is obtained based on the three-dimensional factor graph. The update of information occurs only at the multi-user nodes (MUN) and the decoding nodes (DN). According to [18] and [19], we can define *a posterior* probability log-likelihood ratio (LLR) as

$$\begin{aligned} \gamma(x[j]) &= \text{Log} \frac{\Pr(x_k[j] = 1/r[j])}{\Pr(x_k[j] = 0/r[j])} \\ &= \underbrace{\text{Log} \frac{\Pr(x_k[j] = 1)}{\Pr(x_k[j] = 0)}}_{\lambda^a(x_k[j])} + \underbrace{\text{Log} \frac{\Pr(r[j]/x_k[j] = 1)}{\Pr(r[j]/x_k[j] = 0)}}_{\lambda^e(x_k[j])}. \end{aligned} \quad (14)$$

Then the extrinsic LLR can be derived by

$$\lambda^e(x_k[j]) = \gamma(x_k[j]) - \lambda^a(x_k[j]). \quad (15)$$

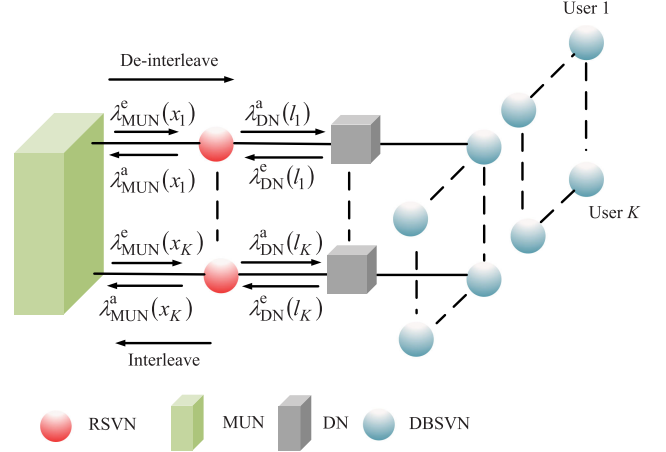


Fig. 3. The three-dimensional factor graph about iterative PIC process of the quantum MU system at the receiving end. (RSVN: Received Sequence Variable Node, DBSVN: Decoded Bit Sequence Variable Node, MUN: Multi-User Node, DN: Decoding Node).

Specifically, the extrinsic LLR of real part of QAM symbol in MUN can be calculated by [20]

$$\lambda_{\text{MUN}}^e(x_k^{\text{Re}}[j]) = \frac{\text{Re}(\tilde{r}[j]) - (\text{E}(\text{Re}(\tilde{r}[j]) - \text{E}(\text{Re}(x[j])))})}{\text{Var}(\text{Re}(\tilde{r}[j]) - \text{Re}(x[j]))}, \quad (16)$$

where

$$\begin{aligned} \text{E}(x_k^{\text{Re}}[j]) &= \frac{\lambda_{\text{MUN}}^a(x_k^{\text{Re}}[j])}{\lambda_{\text{MUN}}^a(x_k^{\text{Re}}[j]) + 1} \cdot 1 \\ &+ \frac{\lambda_{\text{MUN}}^a(x_k^{\text{Re}}[j])}{\lambda_{\text{MUN}}^a(x_k^{\text{Re}}[j]) + 1} \cdot (-1), \end{aligned} \quad (17)$$

and

$$\text{Var}(x_k^{\text{Re}}[j]) = 1 - (\text{E}(x_k^{\text{Re}}[j]))^2. \quad (18)$$

The expression for external LLR of the imaginary part is similar.

In the first iteration, the *a priori* LLR is initialized to 0, that is,  $\lambda_{\text{MUN}}^a(x_k[j]) = 0$ . Through the exchange of the extrinsic LLR between the multi-user node and the decoding node, the information bit sequence of each user is finally obtained in the decoding node through a hard decision. In DN, a standard *a posterior* probability process (APP) that follows the algorithm used in [21] is performed.

Finally, Table I illustrates the steps of the iterative MU PIC algorithm in detail.

### III. SIMULATION RESULTS

This section analyzes the performance of the iterative quantum multi-user system. Furthermore, the EXtrinsic Information Transfer (EXIT) chart is used to evaluate the system's convergence.

In the simulation, we assume that the channel fading is 1. According to [22], we set the wavelength of light as  $\lambda = 1.55 \mu\text{m}$ , the diameter of the receiving aperture as  $D_r = 2 \text{ cm}$ , the distance of link as  $L = 2.5 \text{ km}$ . Moreover, using the previously reported simulation parameters [17], the variance of the thermal noise and the shot noise per photoelectron in the PMT receiver are

TABLE I  
ITERATIVE MU PIC ALGORITHM

<b>1 Initialization:</b> The <i>a priori</i> LLR $\lambda_{\text{MUN}}^a(x_k^t[j])$ , $t \in \{\text{Re}, \text{Im}\}$ is initialized to zero.
<b>2 Iterative PIC Detection:</b>
(1) The extrinsic LLR $\lambda_{\text{MUN}}^e(x_k^t[j])$ can be calculated by Eq. (16).
(2) After deinterleaving, the <i>a priori</i> LLR of DN $\lambda_{\text{DN}}^a(x_k^t[j])$ is obtained.
(3) App decoding is performed in DN and obtain the feedback extrinsic information of DN $\lambda_{\text{DN}}^e(x_k^t[j])$ .
(4) After interleaving, $\lambda_{\text{MUN}}^a(x_k^t[j])$ is generated for multi-user interference estimation in the next iteration.
(5) Go back to step (1) for next iteration.
<b>3 Hard Decision:</b> When the maximum number of iterations is reached, the information bit sequence $\hat{d}_k$ , $k \in [1, K]$ is recovered through hard decision in DN.

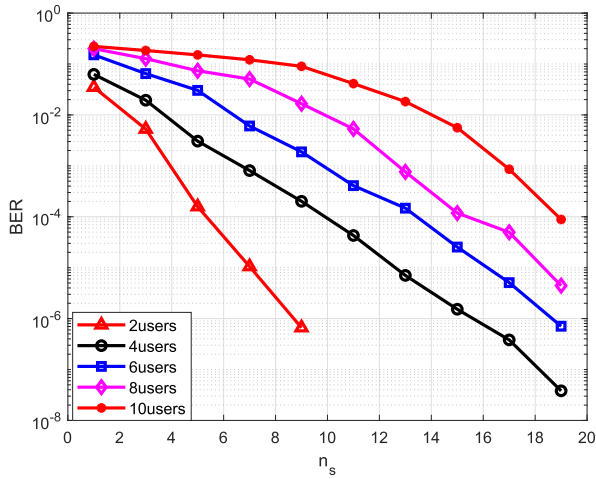


Fig. 4. The BER performance of quantum iterative MU system with quantum mode mismatch of  $\vartheta = 0.9$ , repetition coding rate of  $R_c = 1/8$  for different number of users. In addition, partition numbers are  $2 \times (K + 1)$  and normalized thermal noise of  $\sigma_0/Ae = 0.1$ .

set as  $\sigma_0^2 = 2.56 \times 10^{-26}$  and  $\sigma^2 = \xi^2 A^2 e^2 = 2.56 \times 10^{-24}$ , respectively. Furthermore, the amplification factor of  $A = 10^8$  and spread factor of  $\xi = 0.1$  are used [17].

#### A. Benefit 1: Good Performance in Multi-User Scenarios

Fig. 4 depicts the designed system's BER performance for different number of users. It is observed that as the number of users increases, BER performance deteriorates at the same photon number. However, as shown in Fig. 4, even in the case of 10 users, when the photon number per bit is  $n_s = 19$ , the bit error ratio can reach  $8.8 \times 10^{-5}$ , which shows that the system we designed can well support multi-user communication.

Fig. 5 shows that the BER performance can be improved by the increment of iterations. Quantitatively, For the 4 users scenario, when  $n_s = 15$ , the BER reaches  $10^{-5}$  after 6 iterations while  $10^{-3}$  is obtained for 2 iterations. The reason is that as iteration increases, the more accurate soft LLR can be obtained, which can effectively mitigate the MU interference.

It is also helpful to discuss the computational complexity of the proposed system. In our scheme, it mainly depends on the number of partitions and users, and is expressed by  $O(Q \times N)$ .

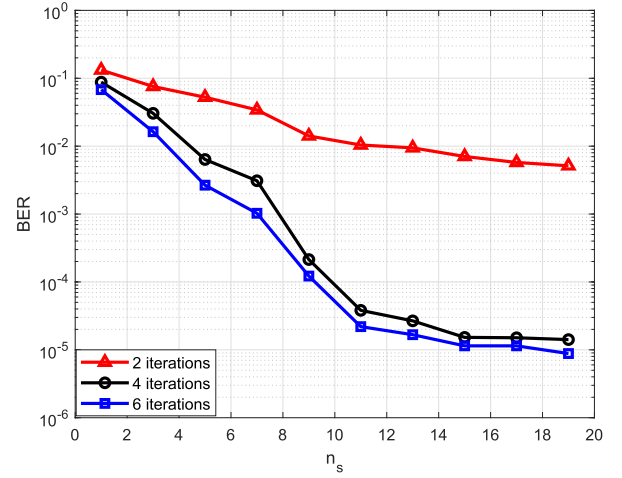


Fig. 5. The BER performance under different iterations for the quantum iterative MU system with 4 users and repetition coding rate of  $1/8$ . Furthermore, partition numbers are set to 10,  $\vartheta = 0.9$  and  $\sigma_0/Ae = 0.1$ .

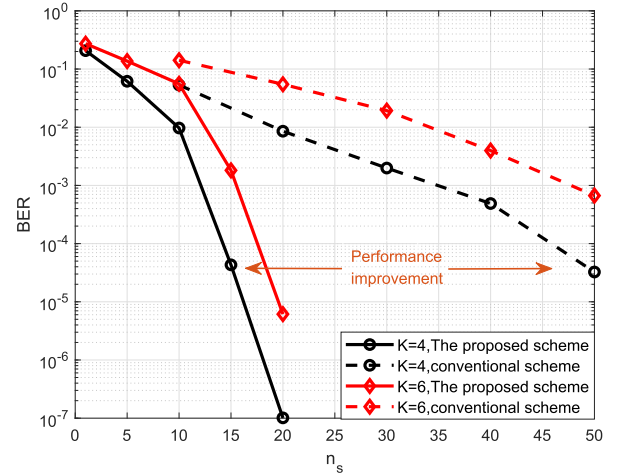


Fig. 6. Comparisons with the conventional photon-counting MU scheme in the case of 4 users and 6 users, for  $R_c = 1/8$ ,  $\vartheta = 0.9$ ,  $\sigma_0/Ae = 0.1$  and partition numbers are  $2 \times (K + 1)$  respectively.

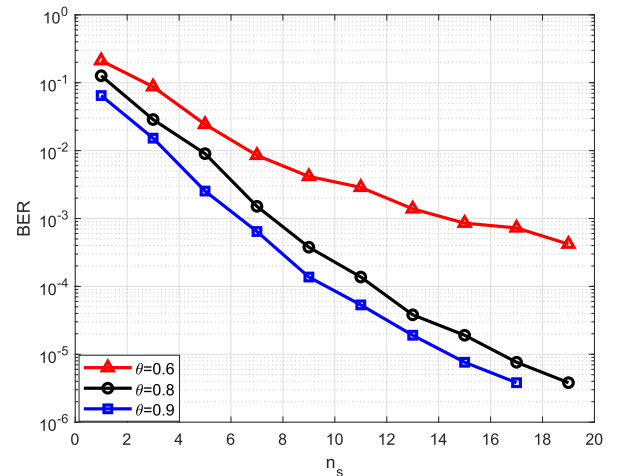


Fig. 7. The BER performance of the proposed system in different mode mismatch, where repetition coding rate is  $1/8$  and partition numbers are 10. Besides, the number of users is fixed at 4 as well as  $\sigma_0/Ae = 0.1$ .

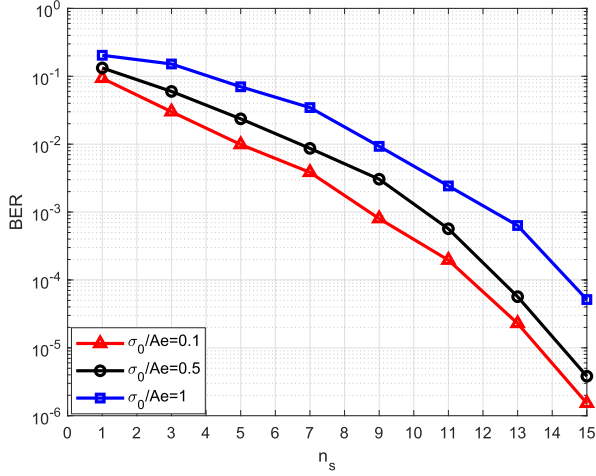


Fig. 8. Impact of the different thermal noise on the quantum iterative MU system. In the simulation, the number of users is fixed at 4 while  $\vartheta = 0.9$  and  $R_c = 1/8$ . In addition, partition numbers are 10.

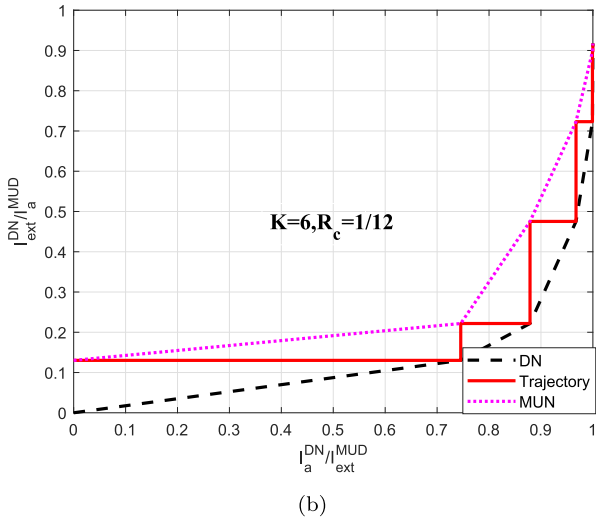
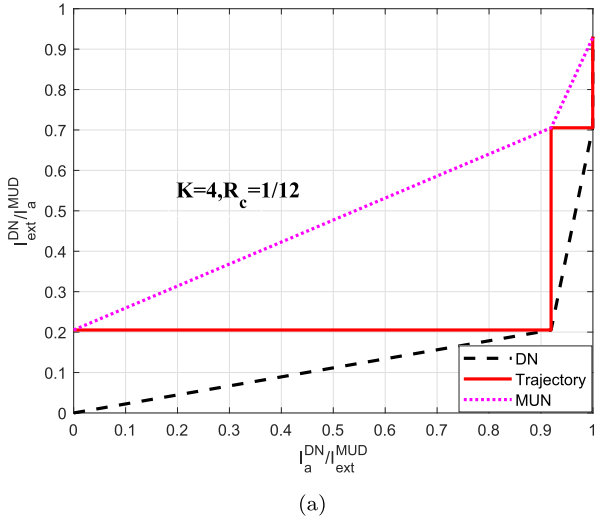


Fig. 9. Normalized EXIT charts of the quantum iterative MU system for (a)  $K = 4$  (b)  $K = 6$ . Furthermore,  $n_s = 10$ ,  $\vartheta = 0.9$ ,  $R_c = 1/12$ ,  $\sigma_0/Ae = 0.1$  and 14 partitions are used in the simulation.

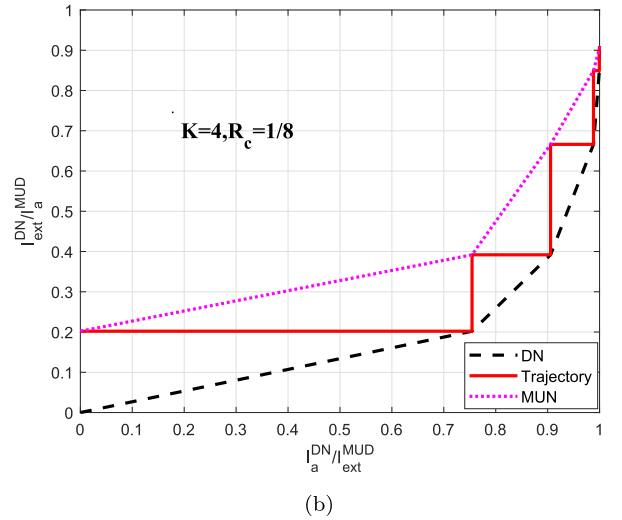
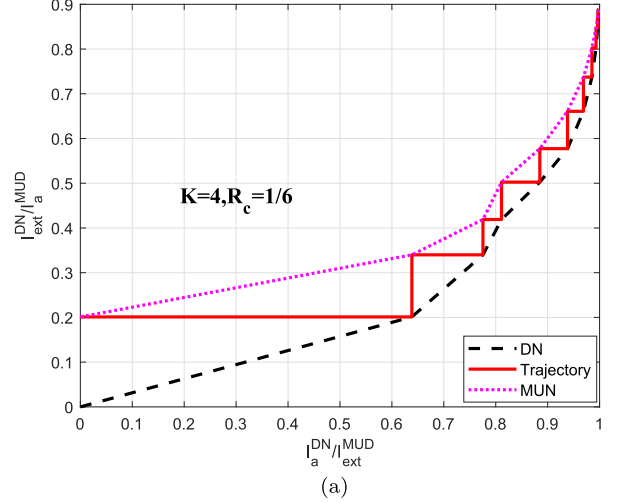


Fig. 10. Normalized EXIT charts of the designed system with  $K = 4$  (4-user) under different coding rate, for  $n_s = 12$ ,  $\vartheta = 0.9$ ,  $\sigma_0/Ae = 0.1$  and 10 partitions. (a).  $R_c = 1/6$ , (b).  $R_c = 1/8$ .

When the number of partitions  $Q$  is set to  $2 \times (K + 1)$ , the overall algorithm complexity is  $O(K^2)$ . This is an acceptable complexity for its good performance.

### B. Benefit 2: Superior Performance Over the Conventional Photon-Counting MU Scheme

It can conclude from Fig. 6 that the designed scheme's performance is greatly improved compared with the conventional photon-counting MU optical code-division multiple-access (OCDMA) scheme [23]. Quantitatively, for the case of  $K = 4$ , the proposed scheme attains a BER of  $1.14 \times 10^{-5}$  at  $n_s = 15$ , while photon numbers per bit of  $n_s = 50$  are needed in the conventional scheme for obtaining the same BER. This is because the composite receiver we developed through the partition detection as possible. Furthermore, MU PIC algorithm is used for soft LLR combining and multi-stage iterative detection, which can further mitigate quantum noise.



### C. Benefit 3: Good Robustness

In practice, various factors can affect system's performance and deteriorate the BER performance. To study the robustness of the system, the following factors are considered: (1) Quantum mode mismatch, (2) Quantum thermal noise.

It can be seen from Fig. 7 that even with mode mismatch, the system has good robustness and can achieve good BER performance. More explicitly, for the  $K = 4$  scenario, even if the mismatch parameter is 0.6 [24], the BER can still reach  $8 \times 10^{-4}$  when  $n_s = 15$ .

According to [17], the BER performance become worse as quantum thermal noise increases when  $\sigma_0/Ae > 0.1$ . However, the system we designed can effectively resist its effect. As shown in Fig. 8, for the  $K = 4$  scenario, when  $\sigma_0/Ae = 1$ , it depicts that the BER of  $5 \times 10^{-5}$  can be obtained at  $n_s = 15$ , showing the superior robustness against quantum thermal noise.

### D. Benefit 4: Fast Convergence

As depicted in Fig. 9, for the case of four users and six users, the proposed system only takes three and five iterations to converge at near (1, 1) point, respectively. It indicates that the designed soft iterative quantum receiver has rapid convergence property. Besides, it can be seen from Fig. 10 that when the code rate is  $\frac{1}{6}$  and  $\frac{1}{8}$  respectively, the iterative receiver needs rounds of 9 and 5 to converge. It shows that the number of iterative rounds required decreases with the lower code rate.

## IV. CONCLUSION

A new quantum coherent-state iterative multi-user communication system is developed in this paper. At the receiving end, we propose the joint quantum multi-stage measurement and iterative MU detection scheme. In particular, under the nonlinear Poisson-Gaussian noise model, an iterative quantum multi-user PIC algorithm is derived. Numerical results indicate that the system we designed can effectively mitigate quantum MU interference and support MU simultaneous transmission with low BER. Besides, it also shows rapid convergence property as well as good robustness about imperfections, e.g. quantum mode mismatch and quantum thermal noise.

## REFERENCES

- [1] A. S. Cacciapuoti, M. Caleffi, R. Van Meter, and L. Hanzo, "When entanglement meets classical communications: Quantum teleportation for the quantum internet," *IEEE Trans. Commun.*, vol. 68, no. 6, pp. 3808–3833, Jun. 2020, doi: [10.1109/TCOMM.2020.2978071](https://doi.org/10.1109/TCOMM.2020.2978071).
- [2] M. B. Rota, F. B. Basset, D. Tedeschi, and R. Trotta, "Entanglement teleportation with photons from quantum dots: Toward a solid-state based quantum network," *IEEE J. Sel. Topics Quantum Electron.*, vol. 26, no. 3, May/Jun. 2020, Art no. 6400416, doi: [10.1109/JSTQE.2020.2985285](https://doi.org/10.1109/JSTQE.2020.2985285).
- [3] C. Liu, C. Zhu, X. Liu, M. Nie, H. Yang, and C. Pei, "Multicarrier multiplexing continuous-variable quantum key distribution at terahertz bands under indoor environment and in inter-satellite links communication," *IEEE Photon. J.*, vol. 13, no. 4, Aug. 2021, Art no. 7600113, doi: [10.1109/JPHOT.2021.3098717](https://doi.org/10.1109/JPHOT.2021.3098717).
- [4] Z. Qu and I. B. Djordjevic, "High-speed free-space optical continuous variable-quantum key distribution based on Kramers-Kronig scheme," *IEEE Photon. J.*, vol. 10, no. 6, Dec. 2018, Art no. 7600807, doi: [10.1109/JPHOT.2018.2875590](https://doi.org/10.1109/JPHOT.2018.2875590).
- [5] L. Hanzo, H. Haas, S. Imre, D. O'Brien, M. Rupp, and L. Gyongyosi, "Wireless myths, realities, and futures: From 3 G/4 G to optical and quantum wireless," *Proc. IEEE*, vol. 100, no. Special Centennial Issue, pp. 1853–1888, May. 2012.
- [6] L. Gyongyosi, S. Imre, and H. V. Nguyen, "A survey on quantum channel capacities," *IEEE Commun. Surv. Tut.*, vol. 20, no. 2, pp. 1149–1205, Apr.–Jun. 2018.
- [7] L. Moli-Sanchez, A. Rodriguez-Alonso, and G. Seco-Granados, "Performance analysis of quantum cryptography protocols in optical earth-satellite and intersatellite links," *IEEE J. Sel. Areas Commun.*, vol. 27, no. 9, pp. 1582–1590, Dec. 2009.
- [8] M. Rezaei and J. A. Salehi, "Quantum CDMA communication systems," *IEEE Trans. Inf. Theory*, vol. 67, no. 8, pp. 5526–5547, Aug. 2021, doi: [10.1109/TIT.2021.3087959](https://doi.org/10.1109/TIT.2021.3087959).
- [9] Z. Li, G. Xu, X. Chen, X. Sun, and Y. Yang, "Multi-user quantum wireless network communication based on multi-qubit GHZ state," *IEEE Commun. Lett.*, vol. 20, no. 12, pp. 2470–2473, Dec. 2016, doi: [10.1109/LCOMM.2016.2610434](https://doi.org/10.1109/LCOMM.2016.2610434).
- [10] K. A. Patel *et al.*, "Quantum key distribution for 10 Gb/s dense wavelength division multiplexing networks," *Appl. Phys. Lett.*, vol. 104, no. 5, 2014, Art. no. 051123.
- [11] Z. Jiang, C. Gong, G. Wang, and Z. Xu, "On the achievable rate and capacity for a sample-based practical photon-counting receiver," *IEEE Trans. Commun.*, vol. 69, no. 9, pp. 6152–6169, Sep. 2021, doi: [10.1109/TCOMM.2021.3088515](https://doi.org/10.1109/TCOMM.2021.3088515).
- [12] D. Zou, C. Gong, and Z. Xu, "Signal detection under short-interval sampling of continuous waveforms for optical wireless scattering communication," *IEEE Trans. Wireless Commun.*, vol. 17, no. 5, pp. 3431–3443, May 2018, doi: [10.1109/TWC.2018.2812161](https://doi.org/10.1109/TWC.2018.2812161).
- [13] J. Ning, G. Gao, J. Zhang, H. Peng, and Y. Guo, "Adaptive receiver control for reliable high-speed underwater wireless optical communication with photomultiplier tube receiver," *IEEE Photon. J.*, vol. 13, no. 4, Aug. 2021, Art no. 7300107, doi: [10.1109/JPHOT.2021.3089781](https://doi.org/10.1109/JPHOT.2021.3089781).
- [14] G. Cariolaro and G. Pierobon, "Performance of quantum data transmission systems in the presence of thermal noise," *IEEE Trans. Commun.*, vol. 58, no. 2, pp. 623–630, Feb. 2010, doi: [10.1109/TCOMM.2010.02.080013](https://doi.org/10.1109/TCOMM.2010.02.080013).
- [15] M. Takeoka and M. Sasaki, "Discrimination of the binary coherent signal: Gaussian-operation limit and simple non-Gaussian near-optimal receivers," *Phys. Rev. A, Gen. Phys.*, vol. 78, no. 2, Aug. 2008, Art. no. 0 22320.
- [16] K. Li, Y. Zuo, and B. Zhu, "Suppressing the errors due to mode mismatch for  $M$ -ary PSK quantum receivers using photon-number-resolving detector," *IEEE Photon. Technol. Lett.*, vol. 25, no. 22, pp. 2182–2184, Nov. 2013.
- [17] D. Zou, C. Gong, and Z. Xu, "Optical wireless scattering communication system with a non-ideal photon-counting receiver," in *Proc. IEEE Glob. Conf. Signal Inf. Process.*, 2016, pp. 11–15.
- [18] X. Yu, X. Zhou, C. Xu, L. Wang, D. Shen, and H. Zhou, "A noma-based quantum key distribution system over poisson atmospheric channels," in *Proc. IEEE Glob. Commun. Conf.*, Waikoloa, HI, USA, 2019, pp. 1–6.
- [19] C. Berrou and A. Glavieux, "Near optimum error correcting coding and decoding: Turbo-codes," *IEEE Trans. Commun.*, vol. 44, no. 10, pp. 1261–1271, Oct. 1996, doi: [10.1109/26.539767](https://doi.org/10.1109/26.539767).
- [20] P. Li, L. Liu, K. Wu, and W. K. Leung, "Interleave division multiple-access," *IEEE Trans. Wireless Commun.*, vol. 5, no. 4, pp. 938–947, Apr. 2006, doi: [10.1109/TWC.2006.1618943](https://doi.org/10.1109/TWC.2006.1618943).
- [21] S. G. Wilson, M. Brandt-Pearce, Q. Cao, and J. Leveque, "Free-space optical MIMO transmission with Q-ary PPM," *IEEE Trans. Commun.*, vol. 53, no. 8, pp. 1402–1412, Aug. 2005, doi: [10.1109/TCOMM.2005.852836](https://doi.org/10.1109/TCOMM.2005.852836).
- [22] T. Özbilgin, M. Koca, "Optical spatial modulation over atmospheric turbulence channels," *J. Lightw. Technol.*, vol. 33, no. 11, pp. 2313–2323, Jun. 2015, doi: [10.1109/JLT.2015.2409302](https://doi.org/10.1109/JLT.2015.2409302).
- [23] L. b. Li, X. Zhou, R. Zhang, D. Zhang, and L. Hanzo, "Performance and capacity analysis of Poisson photon-counting based Iter-PIC OCDMA systems," *Opt. Exp.*, vol. 21, no. 22, pp. 25954–25967, Nov. 2013.
- [24] X. Zhou, C. Wei, D. Shen, C. Xu, L. Wang, and X. Yu, "A shot noise limited quantum iterative massive MIMO system over Poisson atmospheric channels," in *Proc. IEEE Int. Conf. Commun.*, 2019, pp. 1–6.